An Analytic Model of Silicon-based Nanowire Gated Field Effect Transistor Terahertz Signal Detection

Yan Song, Yu Chen, Xuehao Mu, Haijun Lou, Lining Zhang, and Jin He

The Micro- & Nano Electronic Device and Integrated Technology Group, Key Laboratory of Integrated Microsystems, Shenzhen Graduate School of Peking University, Shenzhen, China

Tel: 86-10-62765916 Fax: 86-10-62751789 songyan@ime.pku.edu.cn

Abstract –An analytical terahertz (THz) signal detection model of the Silicon-based nanowire MOSFET (NWFET) is developed in this paper. Beginning from the fundamental hydrodynamic transport equations, the expressions of the velocity spatial distribution and inversion charge transport are obtained. Under the reasonable boundary, an analytical model of the photoresponse of the NWFET is derived out. The comparison between analytical calculation and numerical results confirmed the proposed model. Moreover, the plasma wave transport behavior in the NWFET is analyzed in detail from the presented model and some significant characteristics are demonstrated.

I.. INTRODUCTION

High-quality terahertz (THZ) radiation sources and detectors are the fundamental stone for the development of THZ technology application. Among various techniques, the terahertz radiation and detection based on the two dimensional electron gases oscillation of the gated field effect transistor are drawing much attention for its ability to provide frequency tunable (by voltage), extreme compact (terahertz chip) and room temperature workable THZ source and detectors[1].

The theoretical and numerical analysis had demonstrated that the gated FET with higher mobility and smaller channel length results in good performance of the THZ radiation source and detector [2-11]. The silicon nanowire gated field effect transistor (SNFET), which has been considered to be one of the alternative devices of the traditional bulk CMOS, is expected to be scaled to the shortest channel length theoretically for a given oxide thickness [12-14]. Such a shortest channel also means that the SNFET may be an excellent candidate device for terahertz application. In this paper, an analytical THz detection model for the Silicon nanowire MOS transistor is developed. Starting from the fundamental hydrodynamic equations, the spatial velocity distribution and the inversion charge transport equations are derived. With the appropriate boundary, an analytical model of the photoresponse of the NWFET is obtained. In order to confirm the model prediction, the numerical hydrodynamic simulator is developed and the result is compared with the developed analytical model. Based on these results, the plasma wave behavior in the NWFET structure is analyzed in detail and some unique characteristics are demonstrated.

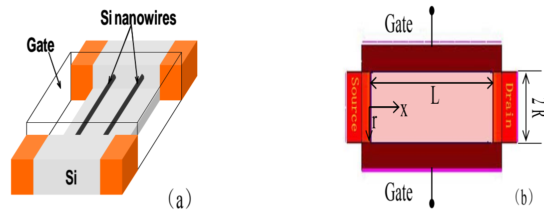

Fig.1 (a) Stereoscopic schematic, (b) cross-section schematic of an N-type SNFET. tox=2nm, R=10nm, Na=1×1017/cm3

II. ANALYTICAL DETECTION MODEL

The structure and coordinate systems of the doped SNFET are show in Fig.1 (a) and (b). The small incoming THz signal is coupled to the source of SNFET by an antenna to induce inversion charge between the source and the gate. In analysis, the incoming THZ signal assumes the formulation of Uacosωt. The generation of the inversion charge is assumed to be able to follow the THz signal change, thus it has the formulation of $Q_a$cosωt, where ω is the THz signal frequency. The oscillating spatial potential will excite the plasma wave along the channel which results in a dc voltage between the source and drain ΔU_{DS}. This dc voltage comparing with the dc gate-to-source voltage $\Delta U_{DS}/U_{GS0}$ is the photoresponse of the THz signal.

Electronic fluid's oscillation in the channel is described by hydrodynamic equation coupled with the continuity equation [2].

$$\frac{\partial v}{\partial t}+v\frac{\partial v}{\partial x}+\frac{v}{\tau_m}=\frac{q}{m}\frac{\partial \phi_s}{\partial x} \quad (1)$$

$$\frac{\partial Q_{in}}{\partial t}+\frac{\partial (Q_{in}v)}{\partial x}=0 \quad (2)$$

Here Q_{in} is the inversion charge density, v(x,t) is the local electron velocity, ψ_s(x,t) is the surface potential and

$\partial\phi_s / \partial x$ is the longitudinal electric field in the SNFET channel, q is the electron charge, m is the effective electron mass of silicon.v/τ_m accounts for electron collision with phonons and electrons, the latter leads to the viscosity of electronic fluid (For the moment, we will neglect the viscosity)

The relationship between variables ψ_s and Q_{in} in the equations above needs to be obtained from the electrostatic analysis of the NWFET. According to electrostatic analysis of the MOSFE device, we have

$$C_{ox}(U_{GS}-\phi_s-\Delta\phi)=(Q_{dep}+Q_{in}) \tag{3}$$

Where $Q_{dep}=qN_aR$ is the depletion charge density in the NWFET; $C_{ox}=\varepsilon_{ox}/R\ln[1+R/t_{ox}]$ is the gate oxide capacitance, $\Delta\psi$ is the work function difference between the gate electrode and intrinsic silicon;

Since the NWFET uses an undoped or lightly doped silicon body in order to enhance the mobility and reduce the threshold voltage fluctuation [13], we can use the fully depletion approximation to simplify the relationship between the inversion charge and the spatial potential. For simplicity we use the symbol $U=U_{GS}-\phi_s-\Delta\phi$ to represent the potential variable, thus, Eq.(3) becomes

$$C_{ox}U=(Q_{dep}+Q_{in}) \tag{4}$$

Differentiate equation (4) with x, we obtain

$$\frac{\partial U(x)}{\partial x}=-\frac{\partial\phi_s}{\partial x}=\frac{1}{C_{ox}}\frac{\partial Q_{in}(x)}{\partial x} \tag{5}$$

Substitute equation (5) into (1), Eqs. (1) and (2) become

$$\frac{\partial v}{\partial t}+v\frac{\partial v}{\partial x}+\frac{v}{\tau_m}=-\frac{q}{mC_{ox}}\frac{\partial Q_{in}(x)}{\partial x} \tag{6a}$$

$$\frac{\partial Q_{in}}{\partial t}+\frac{\partial Q_{in}v}{\partial x}=0 \tag{6b}$$

Boundary condition for equation (6a) and (6b) are

$$Q_{in}(0,t)=Q_c+Q_a\cos\omega t \quad \text{for x=0} \tag{7a}$$

$$j(L,t)=0 \quad \text{for x=L} \tag{7b}$$

Where Q_c is the dc electron sheet density.

Since (6a) and (6b) are nonlinear equations, different harmonics are coupled each other. Under the small signal condition, the solutions of (6a) and (6b) can be written in the following forms:

$$v(x)=v_0(x)+\frac{1}{2}v_1(x)e^{-j\omega t}+\frac{1}{2}v_1^*(x)e^{j\omega t}+..... \tag{8a}$$

$$Q_{in}(x)=Q_{in0}(x)+\frac{1}{2}Q_{in1}(x)e^{-j\omega t}+\frac{1}{2}Q_{in1}^*(x)e^{j\omega t}+..... \tag{8b}$$

Where Q_{in1} is small compared to Q_{in0} and $Q_{in0}(0)=Q_c$. To solve these equations, it first need to find Q_{in1},v_1. Substitute equations (8a) and (8b) into (6a) and (6b) and keep the term vary with ωt, one gets

$$-i\omega v_1(x)+\frac{v_1(x)}{\tau_m}+\frac{q}{mC_{ox}}\frac{\partial Q_{in1}(x)}{\partial x}=0 \tag{9a}$$

$$-i\omega Q_{in1}(x)+Q_c\frac{\partial v_1(x)}{\partial x}=0 \tag{9b}$$

In equation (9a) and (9b), both $\partial Q_{in0}(x)v_1(x)/\partial x$ and $v_0(x)\partial Q_{in1}(x)/\partial x$ terms are neglected and the variation of $Q_{in0}(x)$ with x is out of consideration, which is reasonable since j(L,t)=0. From Eqs. (7a) and (7b), the boundary conditions for (9a) and (9b) become

$$Q_{in1}(0)=\frac{1}{2}Q_a \quad \text{for x=0} \tag{10a}$$

$$j_1(L)=0 \quad \text{for x=L} \tag{10b}$$

Solve equations (9a) and (9b) with boundary conditions (10a) and (10b), one gets

$$v_1(x)=\frac{m\omega C_{ox}}{qQ_cC_0}(k_1e^{iC_0x}-k_2e^{-iC_0x}) \tag{11a}$$

$$Q_{in1}(x)=\frac{mC_{ox}}{q}(k_1e^{iC_0x}+k_2e^{-iC_0x}) \tag{11b}$$

Where

$$k_1=\frac{qQ_a}{2mC_{ox}[1+\exp(2iC_0L)]} \tag{12a}$$

$$k_2=\frac{qQ_a}{2mC_{ox}[1+\exp(-2iC_0L)]} \tag{12b}$$

$$C_0=\pm\frac{\omega\sqrt{mC_{ox}}}{\sqrt{qQ_c}}\sqrt{1+\frac{i}{\omega\tau_m}} \tag{12c}$$

Once the solutions of $v_1(x)$ and $Q_{in1}(x)$ are obtained, the photoresponse of the THZ signal can be derived. Averaging Equation（6a）and （6b）with time over $2\pi/\omega$,one gets

$$\frac{\partial}{\partial x}\left(\frac{|v_1(x)|^2}{2}+\frac{qQ_{in0}(x)}{mC_{ox}}\right)+\frac{v_0}{\tau_m}=0 \tag{13a}$$

$$\frac{\partial}{\partial x}\left(Q_{in0}(x)v_0(x)+\frac{Q_{in1}(x)v_1^*(x)+Q_{in1}^*(x)v_1(x)}{4}\right)=0 \tag{13b}$$

In equation (13a), the term $v_0(x)^2$ is neglected. Boundary condition for (13a) is

$$v_0(L)=v_1(L)=0 \tag{14}$$

Integrate equation (13a) with x from 0 to L and utilize equation (13b), one obtains

$$\frac{q}{mC_{ox}}(Q_{in0}(L)-Q_{in0}(0))=\frac{1}{2}|v_1(0)|^2-\frac{1}{\tau_m}\int_0^L v_0(x)dx \tag{15a}$$

$$v_0(x)=-\frac{Q_{in1}(x)v_1^*(x)+Q_{in1}^*(x)v_1(x)}{4Q_c} \tag{15b}$$

Substitute (11a) (11b) and (15b) into (15a), one gets

$$\frac{Q_{in0}(L)-Q_{in0}(0)}{Q_c}=\frac{Q_{in1}(L)-Q_{in1}(0)}{Q_c}= \frac{1}{4}\left(\frac{Q_{in1}(0)^2}{Q_c^2}\right)\times\left(1+\beta-\frac{1+\beta\cos(2C_0^{'}L)}{\sinh^2(k_0^{"}L)+\cos^2(k_0^{'}L)}\right) \tag{16}$$

Here

$$\beta=\frac{2\omega\tau_m}{\sqrt{1+(\omega\tau_m)^2}} \tag{17a}$$

$$C_0^{'}=\frac{\omega\sqrt{mC_{ox}}}{\sqrt{qQ_c}}\left(\frac{(1+(\omega\tau_m)^{-2})+1}{2}\right)^{1/2} \tag{17b}$$

$$C_0^{"}=\frac{\omega\sqrt{mC_{ox}}}{\sqrt{qQ_c}}\left(\frac{(1+(\omega\tau_m)^{-2})-1}{2}\right)^{1/2} \tag{17c}$$

When τ_m is much small, which is satisfied in silicon material, the higher harmonics are damped out. One could consider that only the plasma wave with fundamental frequency can reach the drain . So equation (16) could be viewed as the detector response. Based on Eq.(4), we have

$$Q_{in0}(0)-Q_{in0}(L)=-C_{ox}(U_0(0)-U_0(L))=C_{ox}U_{DS} \tag{18}$$

Using Eq. (18) in Eq.(16), one obains:

$$\frac{\Delta U_{DS}}{U_{GS0}}=\frac{1}{4}\left(\frac{U_a^{\,2}}{Q_cV_{GS}C_{ox}^{\,2}}\right)\times\left(1+\beta-\frac{1+\beta\cos(2C_0^{'}L)}{\sinh^2(k_0^{"}L)+\cos^2(k_0^{'}L)}\right) \tag{19}$$

NSTI-Nanotech 2009, www.nsti.org, ISBN 978-1-4398-1784-1 Vol. 3, 2009

According to ref[13, 14], the dc electron density Q_{in0} in nanowire is given by

$$U_{GS0}-U_{th0}-\Delta U_{th,VOL}-U_{ch}(x)= \frac{k_BT}{q}\ln[1+\frac{HQ_{in0}(x)}{C_{ox}}]+\frac{k_BT}{q}\ln\frac{qQ_{in0}(x)}{k_BTC_{ox}}+\frac{1}{C_{ox}}Q_{in0}(x) \quad (20a)$$

$$H=q\exp(-q\Delta U_{th,VOL}/k_BT)/k_BT \quad (20b)$$

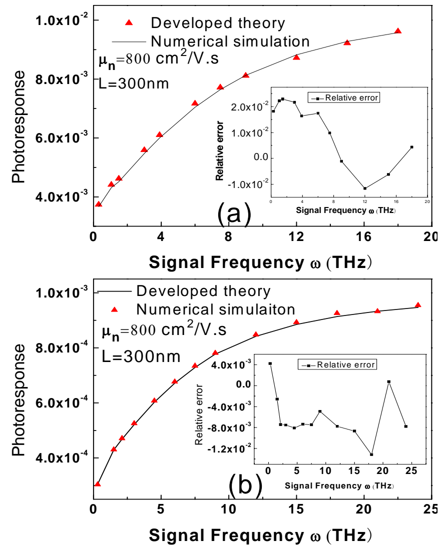

Fig.2 Frequency dependent of photoresponse of SNFET THZ detector with (a) $U_{GS0}=2V$ (b) $U_{GS0}=1V$. The insets in the figure show the relative error.

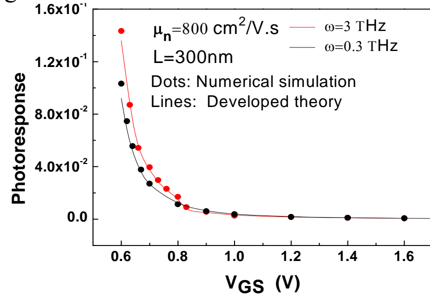

Fig.3 Photoresponse versus gate-to-source voltage

Here $U_{th0}=\Delta\phi+2\phi_f+Q_{dep}/C_{ox}-k_BT/q\ln(4Q_{dep}\varepsilon_{si}/RC_{ox})$ is the transistor threshold voltage similarly to bulk MOSFET, $\Delta U_{th,VOL}=-\frac{k_BT}{q}\ln\frac{q}{2Q_{dep}C_{ox}k_BT}[1-\exp(-\frac{R}{2\varepsilon_{si}k_BT}Q_{dep})]$ is the extra part of threshold voltage, $\phi_f=k_BT\ln(N_a/n_i)/q$ is the Fermi-potential, All the other variables have .their usually meanings.

III. Result and Discussion

Based on the theoretical results, we analyze and discuss the characteristics of the SNWFET as a THz detector. First, by comparing with the numerical model under various conditions, the analytical model is going to be demonstrated to be precise enough to predict the SNWFET's characteristics. Then, using the analytical model, we study the impact of device parameters on the performance of SNWFET terahertz detector and discuss the physical meaning behind it. The numerical model is developed according to Eqs. (6a) and (6b) and the implicit central difference method is used during the numerical calculation [15].

Fig.2 (a) and (b) are the comparison of the photoresponse ($\Delta U_{DS}/U_{GS0}$) versus signal frequency between the model prediction and the numerical simulation for gate-to-source dc voltage equaling to 2V and 1V respectively. Insets in Fig.1 (a) and (b) illustrate

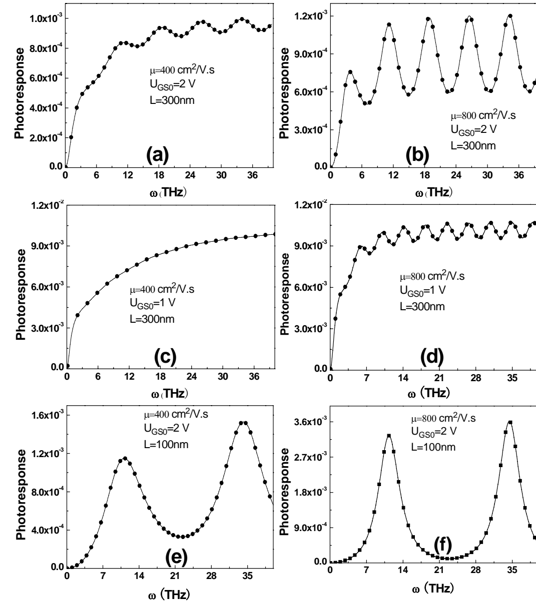

Fig.4 The impact of device length, electron mobility, and dc gate-to-source voltage on the frequency dependent of photoresponse of SNFET THZ detector

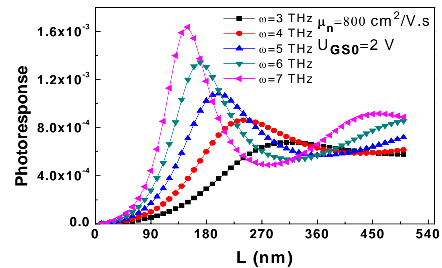

Fig.5 Photoresponse as a function of SNFET channel length.

the relative error between the analytical model and the numerical results. They show that the analytical model is in excellent agreement with the numerical results. The maximum mismatch is less than 1%.

Fig.3 presents the relationship between photoresponse and gate-to-source dc voltage. From the figure, one can see that the analytical model meet very well with the numerical results in general. But when the dc gate-to-source voltage is about 0.6V, the analytical model deviates a little apart from the numerical results. It is reasonable since for $N_a=1e^{17}/cm^3$, the threshold voltage is 0.857 V, which means that SNWFET works in weak inversion region. At this region, the small THz input voltage $U_a=0.05V$ induced an ac electron density comparable to the dc electron density in quantity. Thus this model based on small inversion charge signal approximation is not applicable when $U_{GS0}<0.6V$.

Fig. 4 shows the analytical results of frequency dependent photoresponse of the SNWT THz detector with different gate-to-source voltage, electron mobility, and device length. The fundamental intrinsic frequency of the SNWFET THz detector is given by [14]

$$\omega_0 = \pi s / 2L, \; s = \sqrt{qQ_{in0} / mC_{ox}} \quad (21)$$

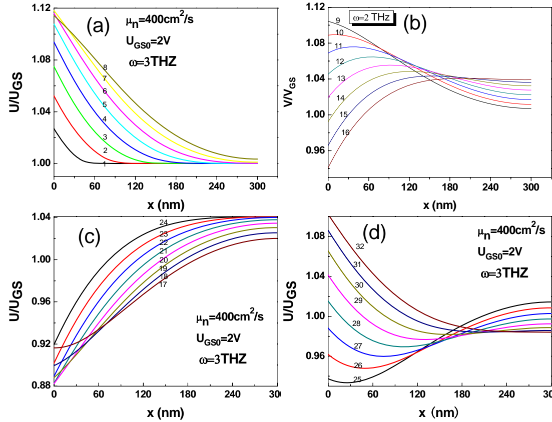

Fig. 6 The induced voltage distribution along SNFET channel with running propagation time in equal intervals

According to Eq (20a), if the external signal frequency $\omega_N = \omega_0(1+2N), \; N = 1,2,3......$, the photoresponse reaches its maximum value, which means the detector working at resonant mode. One can see apparent resonance happening at the detector's fundamental intrinsic frequency and its harmonics in all figures except in Fig. 4 (c). In Fig. 4 (c), the resonance is smeared and vanishes. The quality of the resonance is determined by sτ/L [5]. Comparing these figures, one can find that shortening the length of SNWFET and increasing the electron mobility or U_{GS0} will strengthen the resonance of the SNWFET detector.

Fig 5 presents the analytical results of photoresponse as a function of SNWFET length with different signal frequency. As can be seen in the figure, the photoresponse first rises with L until it reaches a maximum at a certain value. Then the photoresponse begins to drop. With the further increase of L, the photoresponse reaches its second maximum value, which is much small than the previous maximum value. The first maximum point is related to the detector's fundamental resonant frequency and the second is the harmonics. One can also find that with increase of signal frequency, the position of the maximum point moves to the left part of the figure.

In order to show the developing process of plasma wave, we plot the voltage distribution along SNWT channel numerically at different time in Fig.6 (a)-(d). Numbers at the curves indicate their sequence in time. The signal frequency ω equals to3THz. We see clearly in these figure that the oscillation of plasma at the source excited by the incoming THz signal move toward the drain. The amplitude of the plasma wave decrease gradually along the channel, which is due to various scattering mechanism.

Ⅳ Conclusion

In this article, we propose the SNWT to be a THz detector and develop the corresponding detection model. Beginning from the fundamental hydrodynamic transport equations, the expressions of the velocity spatial distribution and inversion charge transport are obtained. Under the reasonable boundary, an analytical model of the photoresponse of the NWFET is derived out. The comparison between analytical calculation and numerical results confirmed the proposed model. Moreover, the plasma wave transport behavior in the NWFET is analyzed in detail from the presented model which shows that the quality of the detector is affected within one oscillation period. Numbers at the curves indicate their sequence in time strongly by electron mobility, dc gate-to-source voltage and device length. Shortening the length of SNWFET and increasing the electron mobility or U_{GS0} will strengthen the resonance of the SNWFET detector and improve the detector quality.

ACKNOWLEDGEMENT

This work is support by the special funds for Micro-Nano Technology Platform of PKU 985 project. The authors would like to thank the numerical tool support from ProPlus Design Solution Inc. (China) and Agilent Inc.

REFERENCES

[1]A. Ei Fatimy et al, "Resonant and voltage-tunable terahertz detection in InGaAs/InP nanometer transistors", Appl. Phys. Lett., vol. 89, p. 131926, 2006.

[2]M. Dyakonov and M. Shur, "Shallow water Analogy for a Ballistic Field Transistor: New Mechanism of Plasma Wave Generation by dc Current", Phys. Rev. Lett, vol 71, p. 2465, 1993.

[3]D. Veksler et al., "Detection of terahertz radiation in gated two-dimensional structures governed by dc current", Phys. Rev. B., vol. 73, p. 125328, 2006.

[4]T. G. Phillips, et al., Proc. " Submillimeter astronomy," Proc. IEEE, vol. 80, p. 1662, 1992.

[5]M. Shur. and M. Dyakonov, " Detection, Mixing, and Frequency Multiplication of Terahertz Radiation by Two-Dimensional Electronic Fluid", IEEE Trans. Electron Devices., vol.43, p. 380, 1996.

[6]J.-Q.L, M. S. Shur, "Terahertz detection by high-electron-mobility transistor: Enhancement by drain bias", Appl. Phys. Lett., vol. 178, p. 2587, 2001.

[7]S. J. Allen, Jr., D. C. Tsui, and R. A. Logan, Phys. Rev. Lett., vol. 38, p. 980, 1977.

[8]W. Knap, et al., J. Appl. Phys., vol. 91, p. 9346, 2002.

[9]F. Teppe, D.Veksler, et al., Appl. Phys. Lett., vol. 87, p. 022102, 2005

[10]A. Ei Fatimy, F, Teppe, N. Dyakonova, W. Knap, D. Seliuta, G. Valusis, A. Shchepetov, Y.Roelens, S. Bollaert, A. Cappy and S. Rumyantsev., , Appl. Phys. Lett., vol. 89, p. 131926, 2006

[11]R.Tauk, et al. , Appl. Phys. Lett., vol. 89, p. 253511, 2006

[12]C. P. Auth et al., IEEE Electron Device Lett., vol. 18, p. 74, 1997.

[13]D. Jiménez et al., IEEE Electron Device Lett., vol. 25, no. 8, p. 571–573, 2004.

[14] Yu Chen, et al., EDSSC'2008, Dec.8-10, Hongkkong, 2008.

[15]C. A. J. Fletcher, "Computational Techniques for Fluid Dynamics", (Springer, New York, 1988